

MICROSTRUCTURES AND MECHANICAL PROPERTIES OF NiAl-Mo COMPOSITES

H. Bei^{1,2} and E. P. George^{1,2}

¹The University of Tennessee, Department of Materials Science and Engineering, Knoxville, TN 37996

²Oak Ridge National Laboratory, Metals and Ceramics Division, Oak Ridge, TN 37831

Abstract

In-situ composites consisting of ~14 vol.% continuous Mo fibers embedded in a NiAl matrix were produced by directional solidification in a xenon-arc-lamp, floating-zone furnace. The fiber spacing and size were controlled in the range 1-2 μm and 400-800 nm, respectively, by varying the growth rate between 80 and 20 mm/h. Electron back-scatter diffraction patterns from the constituent phases revealed that the growth directions and interface boundaries exhibited the following orientation relationships: $\langle 100 \rangle_{\text{NiAl}} // \langle 100 \rangle_{\text{Mo}}$ and $\{011\}_{\text{NiAl}} // \{011\}_{\text{Mo}}$. The temperature dependence of the tensile strength and ductility were investigated and the NiAl-Mo composite was found to be both stronger and have a lower ductile-brittle transition temperature than the unreinforced NiAl matrix.

Introduction

The use of NiAl as a structural material suffers from two major drawbacks: poor ductility/fracture toughness at room temperature and low strength/creep resistance above 600°C. Attempts have been made to toughen NiAl by combining it with a ductile metal [1-11]. For example, Johnson et al. [4] obtained a room-temperature fracture toughness of ~20 MPa $\sqrt{\text{m}}$ in a composite alloy of composition NiAl – 34 at.% (Cr, Mo), and Misra et al. [11] obtained a fracture toughness of ~14 MPa $\sqrt{\text{m}}$ in a NiAl – 9 at.% Mo eutectic alloy. Both these values are significantly higher than the room-temperature fracture toughness of monolithic NiAl single crystals (~6 MPa $\sqrt{\text{m}}$ [12]).

In this study, well-aligned microstructures of NiAl-Mo, devoid of any cellular or dendritic regions, were produced by directional solidification under carefully controlled conditions in a high-temperature optical floating zone furnace having a relatively steep temperature gradient (~30 K/mm). This furnace has been used by us previously to produce well-aligned eutectic microstructures of Cr-Cr₃Si and V-V₃Si alloys over a wide range of growth conditions [13-16].

Experimental Procedures

Alloys having the nominal composition Ni – 45.5Al – 9Mo (at.%) were arc melted, drop cast, and directionally solidified in a high-temperature optical floating zone furnace in flowing argon gas at growth rates of 20-80 mm/h and a fixed rotation rate of 60 rpm. Additional details of the processing conditions are given elsewhere [17]. Total weight losses after melting and casting were less than 0.05%, so nominal (starting) compositions are used throughout this paper.

Representative samples were cut from the directionally solidified (DS) rods along the transverse and longitudinal directions, polished using standard metallographic techniques, etched with a solution of 80% hydrochloric and 20% nitric acids, and examined by optical, electron, and orientation imaging microscopy.

Dogbone-shaped specimens were machined from the DS rods and tensile tested parallel to the fiber direction in vacuum at 25-1000°C and an engineering strain rate of $4.2 \times 10^{-3} \text{ s}^{-1}$. Fracture surfaces were examined in a scanning electron microscope (SEM).

Results and Discussion

Figure 1 shows the well-aligned fibrous microstructure of the NiAl-Mo eutectic obtained by directional solidification at 40 mm/h and 60 rpm where the matrix is the NiAl phase and the continuous fibers are Mo (solid-solution). X-ray microprobe analysis revealed that the NiAl matrix contained essentially no Mo ($< 0.1 \text{ at.}\%$) and had the off-stoichiometric composition Ni-45.2Al, whereas the Mo fibers contained all three elements and had the composition Mo-10.1Al-3.9Ni (all compositions given in at.%). The volume fraction of the Mo fibers was determined to be 0.141.

The arrangement of the Mo rods in the transverse section is approximately hexagonal [Fig.1 (c)], which is the pattern that naturally results at the points of intersection of equal-radius circles drawn around the Mo fibers with each such point equidistant from its neighbors [Fig. 1 (d)]. During steady-state growth, the radius of the circles is determined by the diffusion distance, which in turn is determined by the time available for diffusion (or the directional solidification rate); i.e., the faster the growth rate, the smaller the circles and hence the closer the fiber spacing.

The shape of the individual Mo rods in the transverse section is square rather than circular [Fig. 1(c)], indicating a highly anisotropic NiAl-Mo interfacial energy. Consistent with this, electron backscatter diffraction patterns recorded from the constituent phases at different locations within the as-grown composite revealed the following orientation relationships. The NiAl-Mo interface boundaries were parallel to the $\{011\}$ planes in both NiAl and Mo, whereas, the growth direction was $\langle 100 \rangle$ in both phases.

The $\{011\}$ planes observed in this study are in agreement with those reported previously [11]. These are the closest-packed planes in the BCC and B2 crystal structures of Mo and NiAl [18], and are probably selected during eutectic growth as inter-phase boundaries to minimize the boundary energy. However, the $\langle 100 \rangle$ growth directions observed here are not the same as those reported before [11] where they were found to deviate by $\sim 15\text{-}20^\circ$ from $\langle 100 \rangle$. A possible reason for this difference is that a well-aligned microstructure was obtained in this study whereas a cellular microstructure was observed earlier [11]. When the microstructure is well-aligned, all the Mo fibers are normal to the transverse section (on which the microstructural observations are made). In contrast, the Mo fibers in the cellular structures intersect the transverse section at different angles making it difficult to unambiguously determine the growth direction.

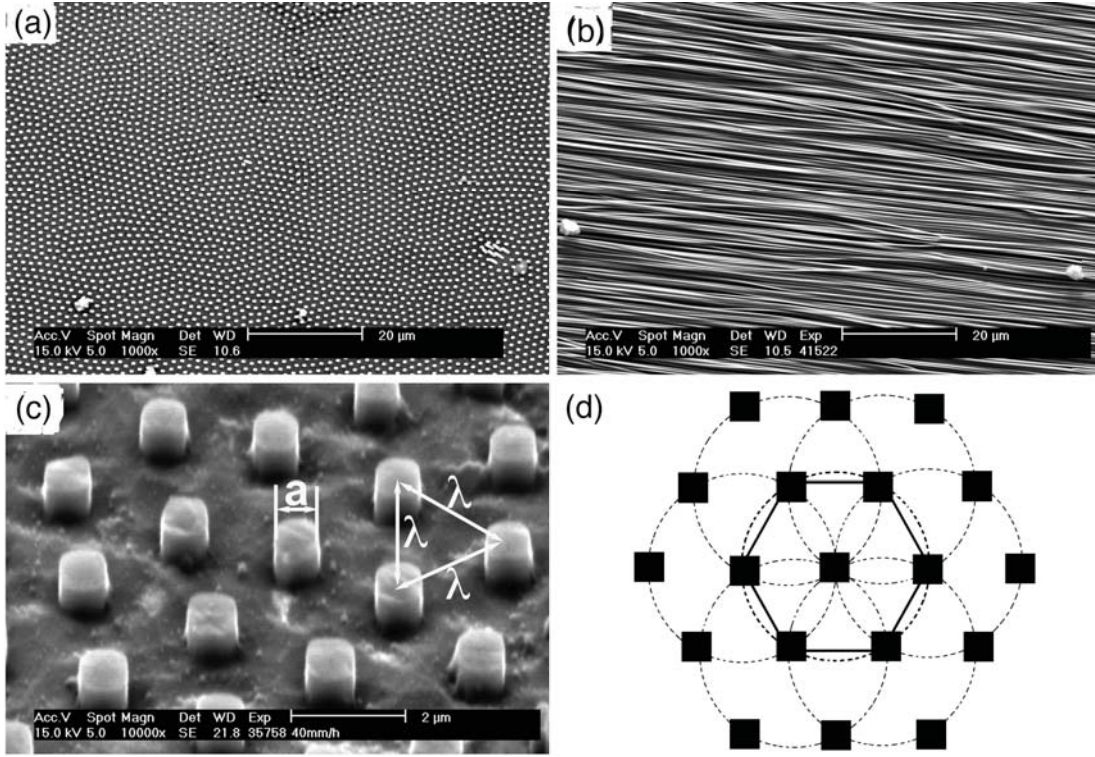


Figure 1. SEM micrographs showing well-aligned rod-like microstructure of the NiAl-Mo eutectic alloy: (a) transverse section, (b) longitudinal section, and (c) higher magnification view of transverse section; (d) schematic of growth mechanism resulting in hexagonal arrangement of Mo fibers.

The fiber spacing, defined as the average distance on a transverse section between the centers of adjacent Mo fibers [λ in Fig. 1(c)], and the fiber size, defined as the average edge length of the square cross-sections [a in Fig. 1 (c)], were measured over a range of growth rates, R , from 20 to 80 mm/h at a fixed rotation rate of 60 rpm. Figure 2 shows examples of microstructures obtained at growth rates of 20 and 80 mm/h.

Jackson and Hunt [19] obtained the following relationship between growth rate R and spacing λ by considering the balance between the diffusion required for phase separation and the energy required for interphase boundary formation:

$$\lambda^2 R = \frac{a^R}{Q^R} = C_1, \quad (1)$$

where Q^R and a^R (and, therefore, C_1) are constants related to the magnitudes of the liquidus slopes at the eutectic temperature, the composition difference between the two phases, their volume fractions, the solid-liquid interface energies of two phases, and the liquid–solid interface shape. Here, C_1 is assumed to have a fixed value over the range of experimental conditions investigated.

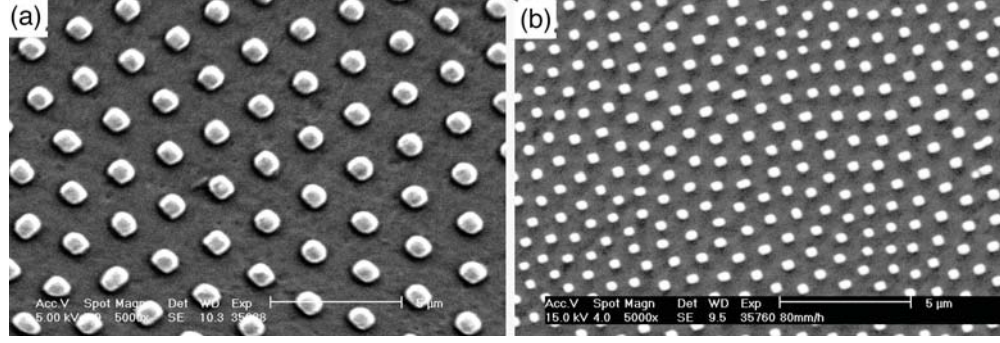


Figure 2. SEM micrographs showing (a) coarse (20 mm/h growth rate), and (b) fine (80 mm/h growth rate) rod-like microstructures in our DS NiAl-Mo alloy.

Since the fiber arrangement on the transverse section is hexagonal, it can be shown that the fiber size (a) is related to the fiber spacing (λ) and the volume fraction of the fibers (V_f) by the following simple expression:

$$a^2 = \frac{\sqrt{3}}{2} V_f \lambda^2, \quad (2)$$

where V_f is constant for a given alloy composition. By eliminating λ from Eqns. (2) and (3) we obtain the following relationship between fiber size and growth rate:

$$a^2 R = C_2. \quad (3)$$

where C_2 is another constant. Therefore, both fiber size and spacing vary inversely as the square root of growth rate [Eqns. (1) and (3)].

Figure 3 is a plot of the experimentally determined values of λ and a versus the reciprocal of the square root of growth rate, \sqrt{R} .

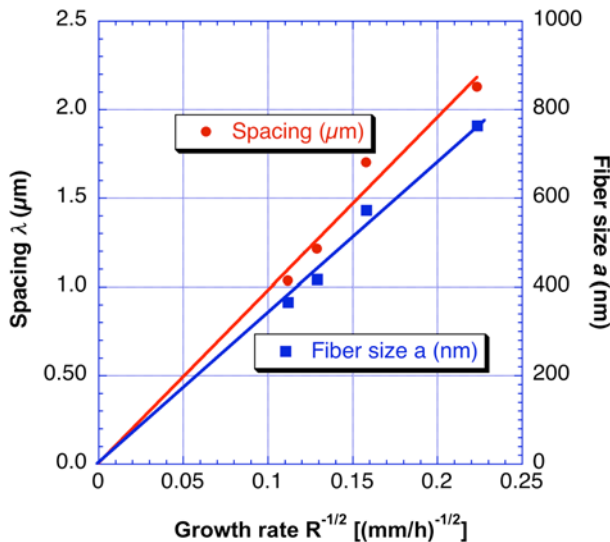


Figure 3. Effects of growth rate on Mo fiber spacing and size in the DS NiAl-Mo alloy investigated in this study.

Consistent with Eqns. (1) and (3) the following linear fits were obtained:

$$\begin{aligned}\lambda R^{1/2} &= 9.76 \mu\text{m} \cdot \text{mm}^{1/2} / h^{1/2} \\ aR^{1/2} &= 3.42 \mu\text{m} \cdot \text{mm}^{1/2} / h^{1/2}\end{aligned}\quad (4)$$

From Eqn. (4), the ratio of fiber spacing to size, λ/a , is found to be 2.85. When this value is substituted into Eqn. (2), the volume fraction of Mo fibers is calculated to be 14.2%, which is in excellent agreement with the measured value of 14.1%.

Tensile tests were performed parallel to the Mo fibers at room temperature and various elevated temperatures to investigate the mechanical properties of the NiAl-Mo composite directionally solidified at 80 mm/h and 60 rpm [microstructure shown in Fig 2 (b)]. Figure 4 is a plot of the 0.2% off-set yield strength and ductility of the composite as a function of temperature. Also included in this figure are the yield strength and ductility of <100>-oriented NiAl having the same composition as the matrix in the composite. The composite has a higher yield strength and lower DBTT than the NiAl matrix.

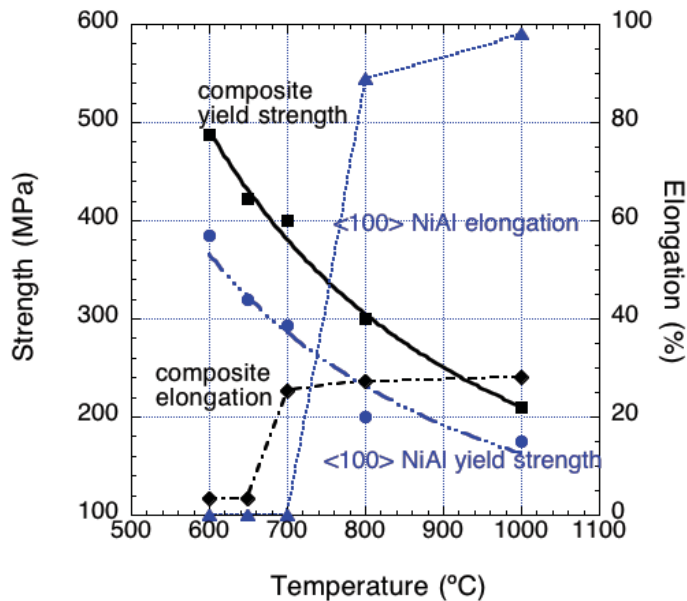


Figure 4. Temperature dependence of the yield strength and ductility of NiAl-Mo composite compared to those of <100> NiAl having the same composition as the matrix in the composite.

Conclusions

Directional solidification in an optical floating zone furnace was used to produce well-aligned rod-like microstructures of NiAl-Mo eutectic alloys. The structures consist of 14 vol.% Mo (solid-solution) fibers having a square cross section embedded in an intermetallic NiAl matrix. The composition of the fibers is Mo-10.1Al-3.9Ni and that of the matrix Ni-45.2Al (< 0.1 Mo). The growth direction is <100> in both the NiAl matrix and the Mo fibers, and the NiAl/Mo interface boundaries are parallel to the {011} planes in both phases. Fiber spacing and size decrease inversely as the square root of the growth rate, and

range from ~1 to 2 μm and ~400 to 800 nm, respectively, for growth rates of 80 to 20 mm/h. When compared to $\langle 100 \rangle$ NiAl single crystals having the same composition as the matrix, the NiAl-Mo composite has higher yield strength and lower DBTT.

Acknowledgment

This research was sponsored by the Division of Materials Sciences and Engineering, Office of Basic Energy Sciences, U. S. Department of Energy, under contract DE-AC05-00OR22725 with UT-Battelle, LLC.

References

- [1] Misra A, Wu ZL, Kush MT, Gibala R, *Materials Science and Engineering A* 1997; 239-240: 75.
- [2] Subramanian PR, Mendiratta MG, Miracle DB, *Metallurgical and Materials Transactions A* 1994; 25: 2769.
- [3] Joslin SM, Chen XF, Oliver BF, Noebe RD, *Materials Science and Engineering A* 1995; 196: 9.
- [4] Johnson DR, Chen XF, Oliver BF, Noebe RD, Whittenberger JD, *Intermetallics* 1995; 3; 99.
- [5] Cline HE, Walter JL, Lifshin E, Russell RR, *Metallurgical Transactions* 1971; 2: 189.
- [6] Subramanian R, Mendiratta MG, Miracle DB, Dimiduk DM, In: Anton DL, Martin PL, Miracle DB, McMeeking R, editors. *Intermetallic Matrix Composites*. Pittsburgh: Materials Research Society 1990. p. 147.
- [7] Frommeyer G, Rahlbauer R, In: George EP, Inui H, Mills MJ, Eggeler G, editors. *Defect Properties and Related Phenomena in Intermetallic Alloys*. Warrendale: Materials Research Society 2003. p. 193.
- [8] Milenkovic S, Caram R, *Mater. Lett.* 2002; 55: 126.
- [9] Milenkovic S, Coelho AA, Caram R, *J Cryst. Growth* 2000; 211: 485.
- [10] Walter JL, Cline HE, *Metall. Trans.* 1970; 1: 1221
- [11] Misra A, Wu ZL, Kush MT, Gibala R, *Philos. Mag. A* 1998; 78: 533.
- [12] Chang KM, Darolia R, Lipsitt HA, *Acta Metall. Mater.* 1992; 40 2722.
- [13] Bei H, George EP, Kenik EA, Pharr GM, *Acta Metall.* 2003; 51: 6241.
- [14] Bei H, George EP, Pharr GM. *Intermetallics* 2003; 11: 283
- [15] Bei H, George EP, Kenik EA, Pharr GM, *Z. Metallkunde* 2004: in press.
- [16] George EP, Bei H, Serin K, Pharr GM, *Mater. Sci. Forum* 2003; 426-432: 4579.
- [17] Bei H, George EP, *Acta Mater.* 2005; 53: 69.
- [18] Villars P, Calvert LD, "Pearson's Handbook of Crystallographic Data for Intermetallic Phases", American Society for Metals, Metals Park, 1985.
- [19] Jackson KA, Hunt JD. *Trans. Metall. Soc. AIME* 1966; 236: 1129.